

Numerical investigations of discrete scale invariance in fractals and multifractal measures

Wei-Xing Zhou ^a, Didier Sornette ^{b,*}

^a*School of Business, School of Science, and Research Center of Systems Engineering
East China University of Science and Technology, Shanghai 200237, China*
^b*D-MTEC, ETH Zurich, CH-8032 Zurich, Switzerland*

Abstract

Fractals and multifractals and their associated scaling laws provide a quantification of the complexity of a variety of scale invariant complex systems. Here, we focus on lattice multifractals which exhibit complex exponents associated with observable log-periodicity. We perform detailed numerical analyses of lattice multifractals and explain the origin of three different scaling regions found in the moments. A novel numerical approach is proposed to extract the log-frequencies. In the non-lattice case, there is no visible log-periodicity, *i.e.*, no preferred scaling ratio since the set of complex exponents spread irregularly within the complex plane. A non-lattice multifractal can be approximated by a sequence of lattice multifractals so that the sets of complex exponents of the lattice sequence converge to the set of complex exponents of the non-lattice one. An algorithm for the construction of the lattice sequence is proposed explicitly.

* Corresponding author. Address: KPL F 38.2, Kreuzplatz 5, ETH Zurich, CH-8032 Zurich, Switzerland. Phone: +41 44 632 89 17, Fax: +41 44 632 19 14.

Email addresses: wxzhou@ecust.edu.cn (Wei-Xing Zhou), dsornette@ethz.ch (Didier Sornette).

URL: <http://www.er.ethz.ch/> (Didier Sornette).

¹ This work was partially supported by the NSFC (Grant 70501011) and the Fok Ying Tong Education Foundation (Grant 101086).

1 Introduction

The word fractal was coined by Mandelbrot to describe sets, which consist of parts similar to the whole and which can be described by a fractal dimension [1], which is in most cases a fractional number. Meanwhile, multifractals were introduced to characterize the statistics of the strength of singularity of self-similar measures carried on general geometric supports [2,3,4,5,6]. Fractals and multifractals have been extensively introduced in the analysis of a wide class of phenomena in physics, geophysics, chemical engineering, turbulence, growth phenomena, and so on. At the same time, new ingredients were added in the theory of multifractals. Based on the discovery of anomalies in DLA (Diffusion Limited Aggregation), the phenomenon of phase transition in the multifractal spectrum was found and studied [7,8,9]. This led to the mathematical framework of the so-called left-sided multifractals [10,11,12,13]. The vector-valued multifractals were introduced to formulate nonconservative measures such as the velocity field of turbulence [14]. Continuous multifractals [15,16,17] were adopted to quantify the droplets breakup in turbulent jet flows [18], which generalize the multipliers from discrete to continuous.

Another important concept is the negative dimension or latent dimension [19,20,21]. The physical implication of negative dimensions was discussed firstly in [22]. In practice, most of the physical processes are random, which leads to the phenomenon of sample-to-sample fluctuations of the multifractal function $f(\alpha)$ by an amount greater than what the error bars on any single sample would indicate. In general, negative dimensions arise in such random multifractals [23,24]. The randomness of multifractals is found at least in two cases where negative dimensions may emerge [23,24]. First, one may obtain a multifractal constructed by a multiplicative cascade that is inherently probabilistic and the negative dimensions, if they exist, describe the rarely occurring events. Second, one may have to investigate the experiment from a probabilistic viewpoint. For instance, one-dimensional cuts of a deterministic measure carried out using a deterministic Sierpinski sponge will inevitably introduce randomness and may be regarded as random samples of a population. It is worth remarking that randomness in multinomial measures does not imply the existence of negative dimensions [25]. Actually, the multifractal slice theorem [26,27] presents a mathematical interpretation of negative dimensions and is the basis of experimental measurement of lower dimensional cuts when the measurement of the whole set is difficult to perform. The multifractal slice theorem makes rigorous some aspects of Mandelbrot's intuition that negative dimensions may be explained geometrically by considering cuts of higher dimensional multifractals.

In the context of fractals and multifractals, scale invariance is the most important concept of symmetry to characterize fractals or multifractal measures. In

its simplest form, scale invariance can be expressed by the following expression:

$$\mathcal{O}(r) = \ell \mathcal{O}(\lambda r), \quad (1)$$

where \mathcal{O} is the observable and λ is the magnification factor or scaling ratio. In the common sense, λ is a continuous parameter resulting in the so-called continuous scale invariance (CSI). In other words, CSI is associated with the fact that expression (1) holds for arbitrary values of λ chosen in the set of positive real numbers. However, CSI is not always true when investigating fractals and multifractals. The general solution to Eq. (1) is not just a power law as CSI would imply but take the form

$$\mathcal{O}(r) = r^{-D} \psi(r), \quad (2)$$

where $D = \ln \ell / \ln \lambda$ is the fractal dimension and $\psi(\lambda r) = \psi(r)$ is a priori an arbitrary log-periodic function with period $\ln \lambda$ [28,29,30,31,32,33] (the term “log-periodic” means that the function ψ is periodic in the variable $\ln r$ with period $\ln \lambda$). Actually, the recently proposed discrete scale invariance (DSI) and its associated complex dimensions are an elaboration of the concept of scale invariance in which that system is scale invariant only under powers of specific values of the magnification factor (see [34] for a review). DSI with the signature of log-periodic oscillations decorating power laws have been reported in several practical applications, such as in material rupture [35,36,37], earthquake precursors [38,39], DLA [40,35], turbulence [41,42,43], and economics [44]. In addition, there are also reports in the theoretical aspects of fractals [28,29,30,31,32,33] and multifractals [45]. Notice the evolution of the concept of dimension from integer to fractional to negative and finally to complex numbers, each time with precise physical meaning.

However, Eq. (1) is only a special (lattice) case of DSI (when λ takes discrete values) [46]. In this work, we shall review the general framework of DSI in strictly self-similar fractals and multifractal measures in Appendix A with extension to joint multifractal measures based on the self-similarity of moments. The structure of the complex exponents will also be discussed for both lattice and non-lattice cases.

The rest of this paper is organized as follows. Extensive numerical simulations are carried out on lattice multifractal measures to investigate different scaling regimes stemming from finite size effects in Sec. 2. We propose a novel approach for the extraction of log-periodicity in the lattice case in Sec. 3. Sec. 4 concludes. The Appendix summarizes the general framework of discrete scale invariance in fractals and multifractals, which is used throughout the paper.

2 Numerical simulations on lattice multifractals

In the absence of analytic results, this section presents computer simulations to explore the properties of lattice multifractal measures. The properties of the log-periodic function $\psi(r)$ are investigated in details. This task remains difficult for lattice multifractals with more than three partitions in each generation. With the increase of partition number n , the iteration number and hence the computational time needed in order to obtain detectable log-periodic structure with relatively low noise level increases exponentially. We thus have to confine our study to small n values. In Sec. 2.1, we study binomial measures with fixed amplification factors $\lambda_1 = (\sqrt{5} + 1)/2$ and $\lambda_2 = (\sqrt{5} + 3)/2$ and varying measure multipliers $m_1 = m$ and $m_2 = 1 - m$ to demonstrate three scaling regimes: the fractal regime, the crossover regime and the Euclidean regime, the latter resulting from finite size effects. Note that the geometric support is not fractal. Then, we study the properties of the Euclidean regime in Sec. 2.2, allowing us to gain insight into the structure of the noise stemming from the incomplete construction of the multifractal measure and of the partitioning. In Sec. 2.3, we study the scaling properties of the amplitude of log-periodic oscillations decorating the scaling of moments.

2.1 Finite size effect

We performed 13 iterations to construct a lattice binomial measure with measure multipliers $m = 0.2$ and $1 - m = 0.8$ (see [47,13,6] for the definition and construction of binomial and multinomial measures). Then the moments $\Gamma(r, q)$ for different orders q were calculated based on the box-counting method with sizes r evenly distributed in logarithmic scale in $[e^{-9}, e^{-1}]$ (see the Appendix for definitions). The log-log plot of $\Gamma(r, q)$ against r for $q = 1$ recovers $\Gamma(r, q = 1) = 1$ (as it should from the normalization of the measure and the definition (A.9) of the moments) with minor fluctuations of order 10^{-15} stemming from the precision of the computation. The log-log plot of $\Gamma(r, q)$ versus r for $q = 0$ is a perfect straight line with slope $-D_0 = -1$. Recall that, if the geometric support is fractal, the slope should be $-D_f$. The log-log plot of $\Gamma(r, q)$ against r for $q \in (0, 1) \cup (1, \infty)$ looks like a strip with slope $\tau(q)$ which is analogous to the situation presented in Fig. 10. We postpone the discussion of this case till Sec. 3.

Fig. 1 shows the dependence of the moments $\Gamma(r, q)$ with respect to box size r in a log-log plot for $q < 0$. There are three regimes clearly visible in the figure separated by two vertical dashed lines. Log-periodic oscillations decorate the scaling law in regime *I*. It is easy to calculate numerically the corresponding log-frequency $f_0 \approx 1/\ln \lambda = 2.0781$ by employing a spectral analysis on the

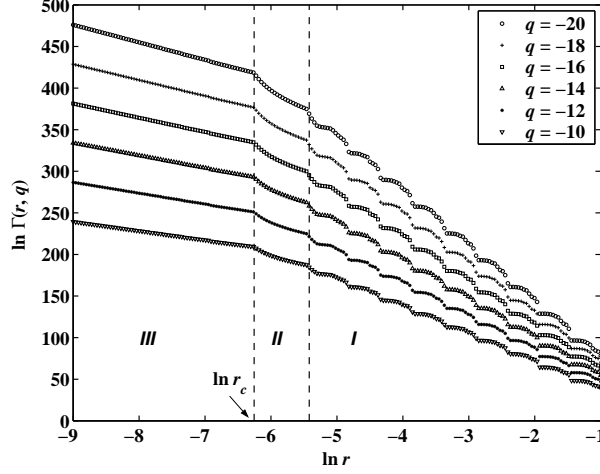


Fig. 1. The dependence of moments $\Gamma(r, q)$ with respect to box size r in a log-log plot for $q < 0$. The multifractal is a lattice binomial measure with scale multipliers $\lambda_1 = \sqrt{\lambda_2} = (\sqrt{5} + 1)/2$ and measure multipliers $m_1 = 1 - m_2 = 0.2$. We performed 13 iterations to construct the multifractal. There are three regimes clearly visible separated by two vertical dashed lines, where I is the fractal regime, III is the Euclidean regimes and II is the crossover regime. The left vertical line is located precisely at $r_c = r_1^{13}$ (see text for details).

residuals defined as $\psi - \langle \psi \rangle$ or on the local derivatives defined in Eq. (A.20) in the Appendix. Regime III corresponds to perfect straight lines with different slopes. Regime II shows the crossover from large box sizes in regime I to small ones in regime III . We shall clarify in the sequel that I is the fractal regime, III is the Euclidean regime and II is the crossover regime. We shall see that this phenomena is due to the finite size effect.

It is well known that, although the mathematical model for the construction of a fractal or multifractal measure contains an infinite number of steps of the iterative construction process, the notion that they are (statistically) self-similar can only apply between certain cutoffs in practice [1]. In other words, what we are able to deal with in nature, laboratory and computer simulations are in fact *pre-fractals* and *pre-multifractals*. We nevertheless use the term “fractal” and “multifractal” without the prefix “pre”, following the custom in the literature.

Let r_c denote the crossover scale (close to the inner cutoff) of a multifractal with measure $\mu_i = \mu(r_i)$ distributed uniformly on a segment \mathcal{F}_i of scale r_i , where $i = 1, \dots, n$. It is clear that

$$r_c = (\max\{r_i\})^b, \quad (3)$$

where b is the iteration number of the construction. This r_c is the largest segment among the n^b segments with uniform measure. Choosing to count boxes with $r < r_c$, we have approximately that $\Gamma(F; r, q) \approx \sum_{i=1}^n \Gamma(\mathcal{F}_i; r, q)$.

There are about $n_i = r_i/r$ boxes covering segment \mathcal{F}_i , each box possessing the measure μ_i/n_i . Thus, we have $\Gamma(\mathcal{F}_i; r, q) = n_i(\mu_i/n_i)^q$. It follows immediately that

$$\Gamma(F; r, q) \approx \sum_{i=1}^n \mu_i r_i^{1-q} r^{q-1}. \quad (4)$$

where $\sum_{i=1}^n \mu_i r_i^{1-q}$ is independent of the box size r . We obtain that $\tau(q) = q - 1$ from the definition (A.15) and $D_q = 1$, corresponding to the Euclidian regime *III*. Concerning the general situation in a d -dimensional space, we have $\tau(q) = (q - 1)d$ and $D_q = d$ in regime *III*. This result just states that a pre-fractal is Euclidean if we investigate it at a very high resolution.

We have observed in Fig. 1 that r_c is precisely the right boundary of the Euclidean regime *III*. The inner cutoff is obviously larger than r_c , since a box with size greater than r_c doesn't guarantee the absence of a possible destruction of the log-periodic structure close to r_c . Indeed, such a box will inevitably split a segment into two parts which introduces errors. However, the inner cutoff can not be determined rigorously but only numerically.

When changing the value of m , we can still observe four different kinds of moments $\Gamma(r, q)$ associated with different q 's: (1) $q < 0$, (2) $q = 0$, (3) $q = 1$ and (4) $q \in (0, 1) \cup (1, \infty)$. It is apparent that the plots of the moments as a function of r for (2) and (3) are similar for all lattice and non-lattice multinomial measures, and thus trivial. For the present binomial measure, when m is large (close to 1), case (1) exhibits a strip while (2) shows three regimes. The results for small m on the three regimes also apply by symmetry $m \rightarrow 1 - m$ to large $m \rightarrow 1$. When $m = (\sqrt{5} - 1)/2$, the measure degenerates to a mono-fractal, where the measure is uniformly distributed over the support with density 1.

2.2 Residuals of the moments in the Euclidean regime *III*

Although regime *III* is trivial in the sense that $\tau(q) = (q - 1)d$, there are still fine structures stemming from those boxes covering two segments and the rightmost box as well. Let us define residuals in regime *III* as

$$\phi(r, q) = \ln \Gamma(r, q) - (q - 1) \ln r. \quad (5)$$

For different $q < 0$, the residuals $\phi(r, q)$ have similar shapes. Figure 2 plots the residual for $q = -20$ with respect to r . We performed $b = 5$ iterations to construct the binomial measure. We see accelerating oscillations with decaying amplitudes towards $r = 0$. The maximal box size is $r_c = 0.0902$. We labelled this point as 0. The consecutive points of local minima and local maxima are labelled as 1, 2, \dots in turn as shown in Fig. 2. The coordinates of these points are denoted accordingly $(r_i, \phi(r_i, q))$ with $i = 0, 1, 2, \dots$. The n -th oscillation

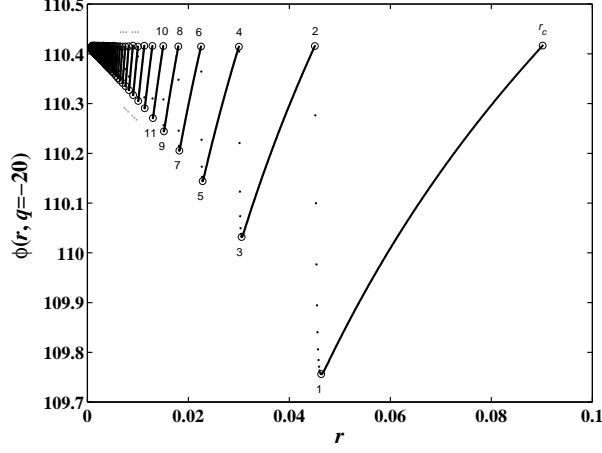


Fig. 2. The dependence of the residual $\phi(r, q = -20)$ defined by expression (5) with respect to r . The even numbers are used to label the points of local maxima, while the odd numbers denote points of local minima. The point 0 is precisely at $r = r_c$. It is visible that $\phi(r_{2n}, q)$ is constant for a given q .

is from point $2n - 2$ through point $2n - 1$ to point $2n$. One can see that the oscillations are similar to each other. We find that

$$\phi(r_{2n}, q) \approx \phi(r_c, q). \quad (6)$$

Note that $r_0 = r_c$. The function $\phi(r_c, q)$ is found to be linear with respect to q with negative slope.

Figure 3 draws the box sizes r_{2n-1} and r_{2n} versus $n + 1$ in a log-log plot. We find the following power laws:

$$r_{2n-1} = 2r_1(n + 1)^{-1} \quad (7)$$

for $n \in \mathcal{Z}^+$ and

$$r_{2n} = r_c(n + 1)^{-1} \quad (8)$$

for $n \in \overline{\mathcal{Z}^-}$. It is important to note that r_{2n-1} and r_{2n} are independent of q for given binomial measures. For different iterations b , r_c and r_1 are not constant anymore. We can determine r_{2n} analytically by combining Eqs. (3) and (8), while r_1 should be calculated numerically for different b . Let $(\delta r)_n = r_{2n} - r_{2n-2}$, then $(\delta r)_n = 1/n(n + 1)$. When $n \rightarrow \infty$, it follows that $(\delta r)_{n+1}/(\delta r)_n \rightarrow 1$, which means that the oscillations are approximately periodic locally for large n . This is not surprised since $(\delta r)_n$ decays more and more slowly when $r \rightarrow 0$ following a $1/n^2$ law.

Define the amplitude of the n -th oscillation as the distance of point $(r_{2n-1}, \phi(r_{2n-1}, q))$ to the line $\phi(r, q) = \langle \phi(r_{2n}, q) \rangle_n$:

$$h_n(q) = \phi(r_{2n-1}, q) - \langle \phi(r_{2n}, q) \rangle_n, \quad (9)$$

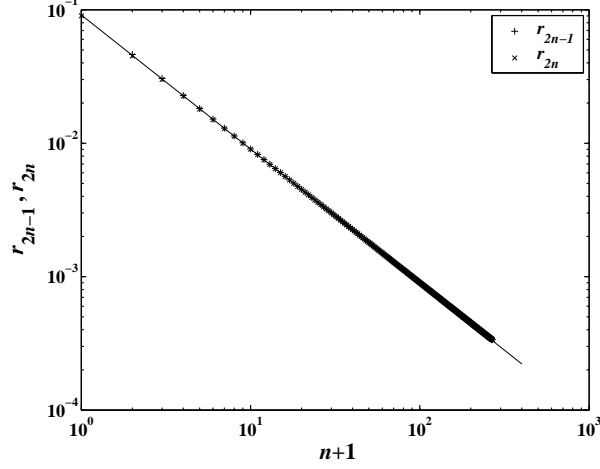


Fig. 3. The power law relationship of r_{2n} (with $n \in \overline{\mathcal{Z}^-}$) and r_{2n-1} (with $n \in \mathcal{Z}^+$) with respect to $n+1$. The scaling exponents are both -1 .

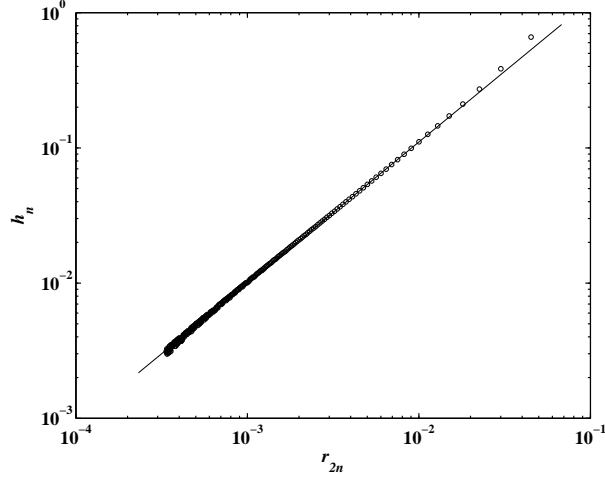


Fig. 4. The power law dependence of the amplitude $h_n(q)$ with $q = -20$ versus r_{2n} . The scaling exponent is $\alpha = 1.0569$.

where $\langle \rangle_n$ is an average over different oscillations n . Figure 4 shows the dependence of the amplitude $h_n(q)$ for $q = -20$ with respect to r_{2n} . Again, we observe a remarkable power law relationship:

$$h_n(q) = c(q) \cdot r_{2n}^\alpha, \quad \alpha = 1.0569, \quad (10)$$

where

$$c(q) = h_1(q)(r_c/2)^{-\alpha} \quad (11)$$

is a function of q .

We also investigated the dependence of $h_1(q)$ with respect to q , as shown in Fig. 5. It seems that $h_1(q)$ approaches a constant when q tends to $-\infty$. The

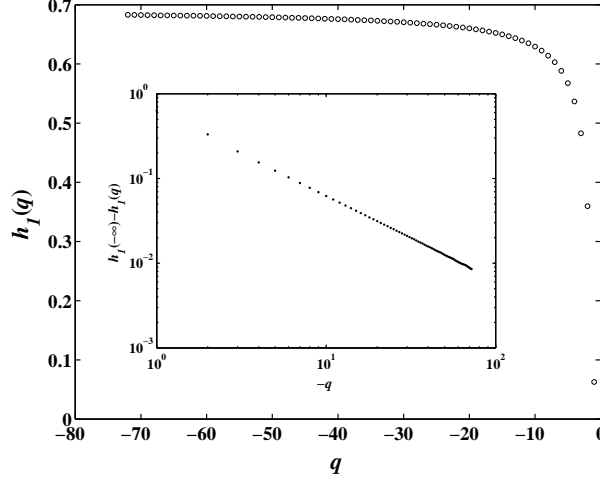


Fig. 5. The dependence of $h_1(q)$ with respect to q . There is a limit for $h_1(q)$ when q tends to $-\infty$. The inset shows the power law dependence of $h_1(-\infty) - h_1(q)$ versus $-q$. The scaling exponent is $\beta = 1.0013$.

points (\circ) in Fig. 5 can be represented by the following law:

$$h_1(q) = h_1(-\infty) - C/|q|^\beta, \quad (12)$$

where the values $h_1(-\infty) = 0.6915$, $\beta = 1.0013$, and $C = 0.6293$ are obtained from a nonlinear regression procedure. The inset verifies the power law dependence of $h_1(-\infty) - h_1(q)$ as a function of $-q$. We also find that $h_1(-\infty) = 0.6915$ is universal for different b and m , while β and C vary for different b and m . In addition, the amplitude $h_1(q)$ increases with $|q|$.

2.3 Residuals of the moments in the fractal regime I

We now study the log-periodic function $\psi(r, q)$ and the corresponding residuals $\ln \psi(r, q) = \ln \Gamma(r, q) - \tau(q) \ln r$ of moments in regime *I* defined in Eq. (A.17) of the Appendix. Denoting $\lambda_1 = \lambda$, we find $\lambda_2 = \lambda^2$. From (A.34), we have $m^q \lambda^{\tau(q)} + (1 - m)^q \lambda^{2\tau(q)} = 1$ which is a solvable univariate second-order equation with respect to $\lambda^{\tau(q)}$. The explicit expression of the exponent $\tau(q)$ follows:

$$\tau(q) = \frac{\ln 2 - \ln \left[m^q + \sqrt{m^{2q} + 4(1 - m)^q} \right]}{\ln \lambda}, \quad (13)$$

where $\lambda = (\sqrt{5} + 1)/2$ is the preferred scaling ratio. The behavior of ψ is simpler, since it is strictly periodic in $\ln r$. Thus, given m and q , the log-periodic oscillations have constant amplitude as a function of r . Figure 6 shows the dependence of $\psi(r, q)$ for $q = -20$ with respect to $\ln r / \ln \lambda$ for different measure multipliers m .

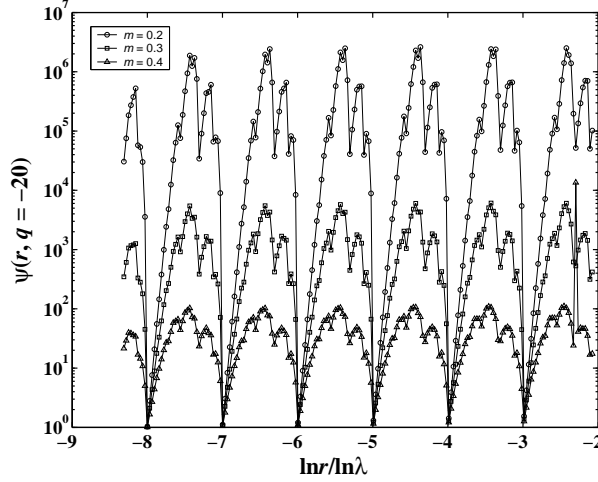


Fig. 6. The dependence of $\psi(r, q)$ for $q = -20$ with respect to $\ln r / \ln \lambda$ for different measure multipliers m . The periodicity is clearly visible with period $\ln \lambda$ in the $\ln r$ variable. The amplitude of the oscillations decreases with increasing m for fixed q . The local minima are located precisely at $r = \lambda^{-i}$ with $i \in \overline{\mathbb{Z}^-}$.

The three lines in Fig. 6 are periodic in $\ln r / \ln \lambda$ with period 1. The amplitudes of the oscillations decrease with increasing m for fixed q . The local minima are located precisely at $r = \lambda^{-i}$ with $i \in \overline{\mathbb{Z}^-}$. The abscissa of the local maxima are different for different m , while those for same m but different q overlap. For large r , the noise increases with m . For small r , the oscillations are gradually spoiled to the right of the crossover regime *II*, which were not shown in Fig. 6. Hence, it is better to investigate the oscillations in the middle of the fractal regime *I* to obtain a quantitative description of the log-periodic oscillations of $\psi(r, q)$.

As shown in Fig. 6, the local minima $\min_r \psi(r, q)$ are close to 1 at $r = \lambda^{-i}$ with $i \in \overline{\mathbb{Z}^-}$. Actually, in the trivial case $r = 1$, the moments $\Gamma(r, q)$ are always equal to 1 for all kinds of conservative multifractal measures and all orders q . We calculated the values of $\min_r \psi(r, q)$ for different q and m . The results are shown in Fig. 7. We find that $\min_r \psi(r, q)$ approaches closer and closer to 1 with the increase of $|q|$ or the decrease of m . The distance of the minima $\min_r \psi(r, q)$ to 1 is exponential as a function of q for fixed m . The slopes of the straight lines fitted to the data for each m in Fig. 7 are approximately evenly spaced for small m . This verifies the analytic results that $\psi(\lambda^{-i}) = 1$.

Figure 8 shows the local maxima $\max_r \psi(r, q)$ versus q for different m . Note that moments of larger m contain a large noise amplitude making the numerical determination of local maxima rather difficult. We find that $\max_r \psi(r, q)$ increases exponentially with $|q|$. This result still holds for other lattice multifractal measures. The slopes of the straight lines fitted to the data for each m in the log-linear plot of Fig. 8 are proportional to $\ln m$.

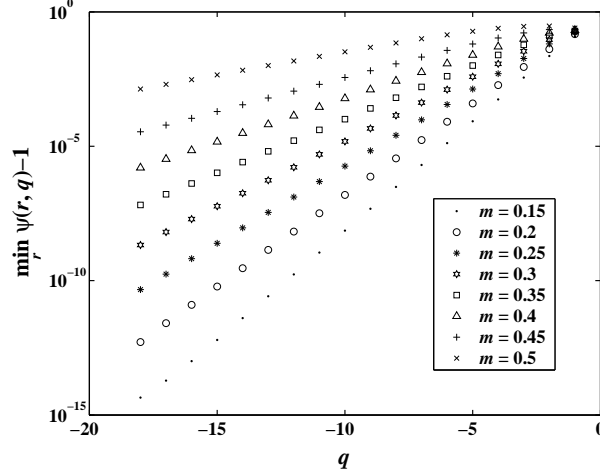


Fig. 7. The exponential approach of $\min_r \psi(r, q)$ to 1 when $|q|$ increases for different m is shown. The slopes of the straight lines are approximately evenly spaced for small m .

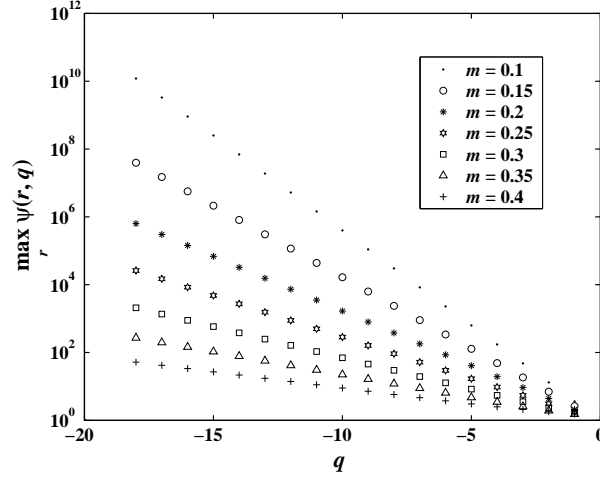


Fig. 8. The exponential dependence of $\max_r \psi(r, q)$ as a function of q for different m . The slopes of the straight lines in this log-linear plot are proportional to $\ln m$.

We define the amplitude of log-periodic oscillations as

$$h(q) = \max_r \psi(r, q) - \min_r \psi(r, q). \quad (14)$$

It is easy to see that $h(q)$ has a behavior similar to that of $\max_r \psi(r, q)$. It follows the important result that the amplitude of the log-periodic oscillations of lattice multinomial measures increases with $|q|$. A similar result is known for (lattice) fractals [30]. This may be related in a qualitative way to the observation that large log-periodic oscillations are found in DLA and in rupture processes compared to very small log-periodic amplitudes in spin models defined on hierarchical geometries. Indeed, fractal growth and rupture processes are controlled by local field / stress concentration, i.e., by the high-order moments of the field involved in the construction of the patterns.

3 A novel approach for extracting log-frequency

A natural question arises in practice concerning the determination of the log-frequency and thus the preferred scaling ratio in the detection of log-periodicity in fractals or multifractals. Up to now, five different methods have attempted to improve the detection of log-periodicity [43]. The common part of four non-parametric methods among the five methods is the Lomb periodogram analysis. The Lomb analysis of $\psi(r, q)$ in Fig. 6 gives a very significant peak at log-frequency $f_0 = 1/\ln \lambda$. Here, we study more complicated measures for which the log-periodic oscillations are not visible to the bare eyes but can still be detected by spectral analysis. We develop in this section a novel method for the detection of log-frequencies, which is expected to be powerful also more generally in the search of log-periodicity in real systems.

We construct a triadic multifractal measure which has three partitions in each generation with scaling ratios $\lambda_1 = 2$ and $\lambda_2 = \lambda_3 = 4$ and measure multipliers $m_1 = m_3 = 0.5$ and $m_2 = 0$. The measure is supported by the generalized Cantor set. Thus the preferred scaling ratio is $\lambda = 2$ and the fundamental log-periodic frequency is $f_0 = 1/\ln 2$. The analytic value of $\tau(q)$ is also given by (13) with $m = 0.5$ and $\lambda = 2$. We use $n = 11$ iterations for the construction of the measure. Again, the counting box size is evenly sampled in the logarithm of the scale. The moments $\Gamma(r, q)$ of the measure were thus calculated for different orders q based on the box-counting method.

We present in Fig. 9 a typical plot of $\ln \Gamma(r, q)$ versus $\ln r$ for $q < 0$. Although the plot is very noisy, a linear least square fitting gives a slope close to the analytic exponent $\tau(q)$. No unambiguous simple (log-)periodic oscillations are visible. Since $\ln r_c = -n \ln \lambda_1 = -7.62$, we restricted the interval of study to $-6.17 < \ln r$, where the lower bound is indicated by the left downward arrow in Fig. 9. Indeed, a behavior different from large r can be observed for small r . We also introduced an outer cutoff in the large r range as indicated by the right upward arrow in Fig. 9. Our analysis for the detection of log-periodicity was thus carried out in the interval confined within the two arrows, containing a total of $N = 131$ data points. Note that a different but reasonable choice of this interval doesn't impact on the results.

Fig. 10 shows a typical plot of $\ln \Gamma(r, q)$ versus $\ln r$ for $q > 1$. A linear least square fit of the points recovers a numerical estimate of $\tau(q)$ which is close to the theoretical value. The plot also exhibits many parallel patterns (rectangle-like) which are arranged periodically in $\ln r$, as indicated by the arrows. We find that the period is approximately $2 \ln \lambda$, which is interpreted as the frequency of a subharmonic to the fundamental log-frequency. A similar subharmonic log-periodic frequency was also reportedly detected in the growing diffusion-limited aggregation clusters [40]. However, the Lomb periodogram of

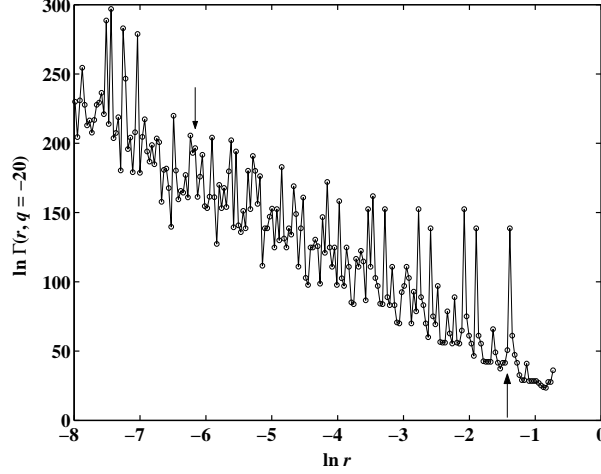


Fig. 9. The dependence of $\ln \Gamma(r, q)$ with respect to $\ln r$ for $q = -20$. Although the plot is very noisy, a linear least square fitting gives a slope close to the analytic exponent $\tau(q)$. No unambiguous (log-)periodic oscillations are visible.

the detrended $\ln \Gamma(r, q)$ in Fig. 10 doesn't provide convincing signal of such $f_0/2$ subharmonic (not shown). We nevertheless observed in the Lomb periodogram two outstanding peaks at log-frequencies $f = 11.54$ and $f = 15.87$, although this observation does not ensure the statistical significance of log-periodicity. Lower order moments provide more significant Lomb periodogram when $q > 0$, which means that the noise was amplified rapidly for large q 's. On the other hand, the impact of q on the noise is less important when $q < 0$. This noise amplification effect of larger q suggests to investigate lower-order moments to detect log-periodicity.

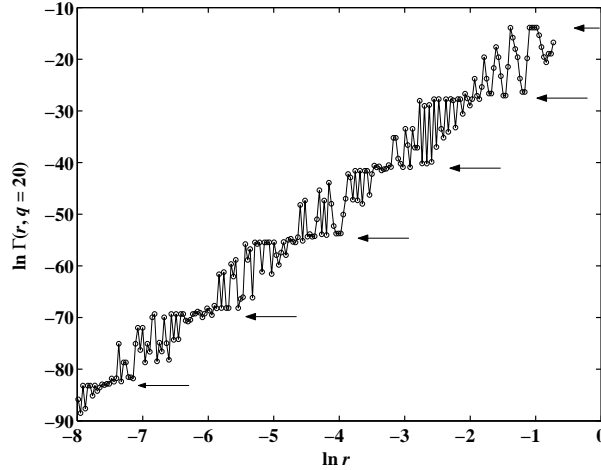


Fig. 10. The dependence of $\ln \Gamma(r, q)$ with respect to $\ln r$ for $q = 20$. The arrows indicate a periodic pattern in $\ln r$. The period is $2 \ln \lambda$ which is interpreted as a subharmonic of the fundamental log-frequency.

We detrended the moment $\ln \Gamma(r, q = -3)$ to remove the power-law scaling. Here the scaling exponent is estimated directly from the data points and the

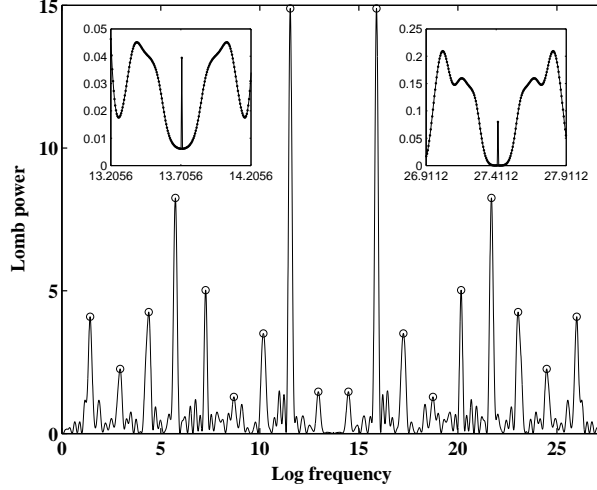


Fig. 11. The Lomb periodogram of the residuals of the $q = -3$ order moment. The left inset shows the local details around $f = 9.5/\ln \lambda$, which is the symmetric axis of the periodogram. The right inset shows the local details around $f = 19/\ln \lambda$, beyond which the Lomb periodogram duplicates itself periodically. The Lomb peaks indicated by open circles are approximately evenly spaced.

resultant residuals have zero mean. This method was used extensively in practice (this method is different from that used in Sec. 2.2 and 2.3). Analyzing these residuals by the Lomb method gives a Lomb periodogram shown in Fig. 11. It is interesting to point out that the Lomb periodogram is periodic of period $19/\ln \lambda = 27.4112$. The local detail around $f = 27.4112$ is shown in the right inset of Fig. 11. We see a clear burst exactly at $f = 27.4112$ causing the discontinuity at this point. It is necessary to stress that this burst itself is not a Lomb peak. It is thus sufficient to analyze only the $f < 27.4112$ part of the periodogram as shown in Fig. 11. In addition, the Lomb periodogram in Fig. 11 is apparently symmetric with respect to $f = 9.5/\ln \lambda = 13.7056$. The left inset shows the local detail around $f = 13.7056$, which is a discontinuous burst as well. This is the reason why the right inset is symmetric with respect to $f = 27.4112$.

In Fig. 11, the two highest peaks are located at $f = 11.54$ and $f = 15.87$. This is what we can see in the Lomb periodogram for $q > 1$ as we alluded above. The claim that the fundamental logarithm frequency is $f_0 = 11.54$ or $f_0 = 15.87$, as done in many other practical systems, has a false-alarm probability of 0.006% assuming that the noise is independent and Gaussian [48,49]. The existence of two peaks of the same height and the symmetric structure of the Lomb periodogram reinforce further the statistical significance of the existence of a genuine log-periodicity.

An additional important evidence is offered by expanding $\psi(r, q)$ in the Fourier space, which identifies a discrete set of log-frequencies f_n with amplitudes A_n . Here, we find that the amplitudes A_n of different frequencies f_n are not

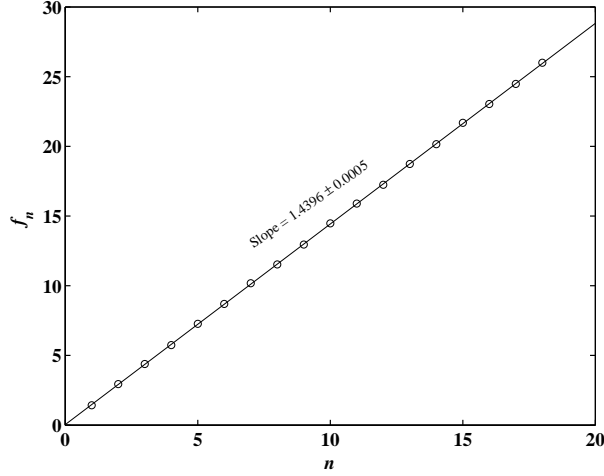


Fig. 12. The linear dependence of log-frequencies f_n of the harmonics of the fundamental frequency f_0 as a function of their order n . The slope of the fitted straight line is 1.4396 ± 0.0005 providing an estimate of f_0 in excellent agreement with the theoretic value of $f_0 = 1/\ln 2$. The preferred scaling ratio is thus $\lambda = 2.0030 \pm 0.0005$ having only a 0.3% deviation from the true value of $\lambda = 2$.

restricted to a presumed inequality that $A_1 > A_n$ with $n > 1$ (we refer to [50] for a detailed discussion). In the case where several A_n are comparable, as shown in Fig. 11, we have to study the harmonics of the fundamental frequency. There are indeed many slim peaks in Fig. 11 that are approximately evenly spaced. We indicated these 18 peaks with open circles, whose corresponding log-frequencies are denoted as f_n . This recognition process is objective, since all except the 6th and 13th peaks are higher than the remaining peaks. It is quite reasonable to interpret f_n as the n -th harmonic of the fundamental log-frequency. A convenient estimate of f_0 is the mean of the differences of consecutive frequencies. This gives $f_0 = \langle f_n - f_{n-1} \rangle = 1.4457 \pm 0.0671$. In addition, we can expect that $f_n \approx n f_0$. Thus, we can take the slope of the line fitted to points (n, f_n) as another estimate of f_0 . Figure 12 plots f_n as a function of n , which exhibits an almost perfect linear relationship. The slope of the fitted line is $f_0 = 1.4396 \pm 0.0005$. The estimates of f_0 from the two approaches are comparable to each other and both in excellent agreement with the theoretic value of $f_0 = 1.4427$. However, the linear regression method of Figure 12 is obviously much more stable. The preferred scaling ratio is thus calculated to be $\lambda = e^{1/f} = 2.0030$ with a standard deviation $\sigma_\lambda = \sigma_f e^{1/f} / f^2 = 0.0005$.

In real systems, it is possible that the Lomb periodogram is much more noisy than found in Fig. 11. In that case, we may only determine a few but not all harmonics, so that the successively detected harmonics are not consecutive. In this case, taking the differences between successively detected harmonics will not give a constant value equal to the fundamental log-frequency. This certainly increases the difficulty of the detection of log-periodicity and low-

ers the significance of the extracted log-frequency. One should thus estimate subjectively the possible order of the detected harmonics and reconstruct the best match according to a linear fit such as in Figure 12 but with holes for the missing harmonics. Notwithstanding its difficulties, this method was successfully applied to the search of log-periodicity in the energy dissipation of three dimensional fully developed turbulence [43].

4 Concluding remarks

We have reviewed and generalized in this paper the basic discrete scale invariance equations concerning the moments $\Gamma(r, q)$ of fractals, multifractal measures and joint multifractal measures based on the presence of (statistical) self-similarity in these objects. There exist a set \mathcal{T} of complex dimensions for fractals and complex exponents for multifractals, corresponding to the set of complex solutions of the corresponding DSI equation (DSI: discrete scale invariance). The set \mathcal{T} lies in a strip $[\tau^R(q), \tau_0(q)] \times \mathcal{R}$ in the complex plane and is symmetric with respect to the real axis, where $\tau^R(q) \in \mathcal{T}$ is the only exponent on the real axis.

In the lattice case, the complex exponents are located evenly with spacing ω (where ω is the fundamental angular log-frequency) on finitely many vertical lines in the complex plane. Corresponding to the complex exponents on the vertical line $\tau(q) = \tau^R(q)$, there is a log-periodic expression of $\Gamma(r, q)$ with a fundamental log-frequency $f = 1/\ln \lambda$, where λ is the preferred scaling ratio. We have verified the log-periodicity in multifractals numerically and proposed a novel precise approach for the extraction of f . Our simulations also show that the signal-to-noise ratio of the moments increases with $|q|$ when $q < 0$ or $q > 0$. Since larger signal-to-noise ratio corresponds to more significant Lomb peak, we should investigate lower-order moments to extract log-frequencies, which is independent of the fact that higher-order moments have larger amplitudes of oscillations.

In the non-lattice case, the complex exponents are irregularly located in the strip and $\tau^R(q)$ is the unique complex exponent in the vertical line $\tau(q) = \tau^R(q)$. There are thus no preferred scaling ratio and no exact log-periodicity. However, we can construct a sequence of lattice multifractals whose preferred scaling ratios converge to 1 from above to approximate the non-lattice multifractal so that the set of these lattice multifractals converge to the set of complex exponents of the non-lattice multifractal. In the Appendix, we propose an explicit algorithm for the construction of the lattice sequence.

Therefore, we can recognize lattice fractals and/or multifractals in real systems from the evidence of the presence of log-periodicity. We can obtain a preferred

scaling ratio λ based on spectral analysis. This search not only sheds new light towards a better understanding of the system under study but also offers a constraint on the modelling of the system. Of course, λ does not contain a detailed information on all the scaling ratios λ_i . It should be noted that the search for log-periodicity has been carried out already in several real systems, such as in the growing diffusion-limited aggregation (DLA) clusters [40], in two dimensional free decaying turbulence [42] and in three dimensional fully developed turbulence [51,43]. It is interesting that the preferred scaling ratio is $\lambda \approx 2$ for the cases of DLA and 3D turbulence and it is possible that the log-frequency $f_0 = 4 \sim 5$ in the two dimensional free decaying turbulence case [42] turns out to be a harmonic of $f_0 = 1/\ln 2$. However, we have to stress that the existence of a preferred scaling ratio λ does not imply that there is only one scaling ratio equal to the measured λ . For instance, $\lambda = 2$ found in 3D turbulence does not mean that the p -model [52] is the correct and only one model. We shall further clarify this point by taking the growing DLA clusters as an example as follows.

There are many models proposed to explain the fractal growth of DLA clusters, such as the hierarchical ghost model [53,54] and the Fibonacci model [55,56,57]. In the hierarchical ghost model, pairs of single particles collide and aggregate to form dimers. Then pairs of dimers collide and aggregate to form four-particle clusters. This hierarchical growth process goes on and on to form eventually a large DLA cluster. Defining $b(N)$ as the average number of bonds along the connecting pathway between two particles on an N -particle cluster, we obtain the DSI equation [53]

$$b(2N) = \frac{3}{2}b(N). \quad (15)$$

Since the average radius R of a N -particle cluster obeys $R \sim \sqrt{b(N)}$ and $N \sim R^D$, we have $D = 2 \ln 2 / \ln(3/2)$ and the set of complex exponents with respect to (15) is

$$\mathcal{T} = \{2/D + 2\pi ni / \ln 2, \ n \in \mathcal{Z}\}. \quad (16)$$

It is clear that $\lambda = 2$ and the set of complex exponents is on a vertical line with abscissa of $2/D$ in the complex plane. On the other hand, by applying the results of the wavelet transform modulus maxima (WTMM) representation to the DLA azimuthal Cantor set, it follows that the number $N(a)$ of maxima of the WTMM skeleton at scale a satisfies the Fibonacci rule [55,56,57]:

$$N(a) = N(\lambda a) + N(\lambda^2 a). \quad (17)$$

It is easy to show that the set of complex dimensions is [40,46]

$$\mathcal{D} = \left\{1 + \frac{\ln \phi}{\ln \lambda} + i \frac{2\pi n}{\ln \lambda}\right\} \cup \left\{1 - \frac{\ln \phi}{\ln \lambda} + i \frac{(2n+1)\pi}{\ln \lambda}\right\}, \quad (18)$$

where $n \in \mathcal{Z}$ and $\phi = (\sqrt{5} + 1)/2$ is the golden mean. We see that there are two vertical lines in the complex plane in this model. Numerical simulations [40] lead to the identification of two log-frequencies $f_0 = 1/\ln \lambda$ and $f_0/2$ in excellent agreement with the prediction of the Fibonacci model. The preferred scaling ratio was estimated numerically to be $\lambda = 2.2$. It shows that the Fibonacci model with two scaling ratios λ and λ^2 provides a better description than the hierarchical ghost model in the sense of discrete scale invariance.

A General framework of discrete scale invariance in fractals and multifractals

In this Appendix, we revisit the equations governing the concepts of discrete scale invariance (DSI) and the associated complex exponents in fractals and multifractal measures, and generalize them to joint multifractal measures. We shall show that the set of complex exponents lie symmetrically with respect to the real axis in a vertical strip in the complex plane. Furthermore, in the lattice case, the set of complex exponents lie on finitely many vertical lines periodically and the DSI leads to the log-periodic corrections to scaling implying a preferred scaling ratio that is proved to be independent of the order of the moments. In the non-lattice case, there are no visible log-periodicity, *i.e.*, no preferred scaling ratio since the set of complex exponents are spread irregularly within the complex plane. A non-lattice multifractal can be approximated by a sequence of lattice multifractals so that the sets of complex exponents of the lattice sequence converge to the set of complex exponents of the non-lattice one. An algorithm for the construction of the lattice sequence is proposed explicitly.

A.1 Revisiting DSI in fractals

Smith et al [30] studied three Cantor sets with the initiators being 101 (the classic Cantor set), 101001001, and 101010001. They followed the Grassberger-Procaccia (G-P) approach [58] and investigated the periodic oscillations in the log-log plot of the correlation integral $C(\ell)$ with respect to scale ℓ . In this section, we revisited DSI in the classic Cantor set using an alternative approach [28].

In order to generalize to other self-similar fractal sets, consider a fractal set \mathcal{F} , which is the union of n disjoint parts \mathcal{F}_i , namely $\mathcal{F} = \cup_{i=1}^n \mathcal{F}_i$ with $\mathcal{F}_i \cap \mathcal{F}_j = \emptyset$ for $i \neq j$. Let $N(\mathcal{F}; r)$ be the number of boxes covering \mathcal{F} with scale r . We assume that the magnification of \mathcal{F}_i by a factor λ_i results in \mathcal{F} . This leads to

$$N(\mathcal{F}_i; r) = N(\mathcal{F}; \lambda_i r). \quad (\text{A.1})$$

Note that the reciprocal of the amplification factor, $1/\lambda_i$, is called the scale multiplier. Since

$$N(\mathcal{F}; r) = \sum_{i=1}^n N(\mathcal{F}_i; r), \quad (\text{A.2})$$

we obtain

$$N(\mathcal{F}; r) = \sum_{i=1}^n N(\mathcal{F}; \lambda_i r), \quad (\text{A.3})$$

Equation (A.3) has a solution if and only if there exist integers k_i and λ satisfying

$$\lambda_i = \lambda^{k_i}, \quad (\text{A.4})$$

which is the generalization of the Fibonacci rule of the number of maxima of the WTMM skeleton at a given scale in diffusion-limited aggregation [40] and corresponds to the so-called lattice case [46]. The solution can be expressed as

$$N(\mathcal{F}; r) = r^{-D} \psi(r). \quad (\text{A.5})$$

where $\psi(r) = \psi(\lambda r)$ and D is the fractal dimension determined by the real solution of equation

$$\sum_{i=1}^n \lambda_i^{-D} = 1. \quad (\text{A.6})$$

We see that $N(\mathcal{F}; r)$ exhibits log-periodic oscillations with respect to r . Since $N(\mathcal{F}, 1) = 1$, it follows that $\psi(\lambda^{-\ell}) = 1$, where $\ell \in \overline{\mathbb{Z}}^-$. For $k_i = 1$, we recover Eq. (1).

A.2 DSI in multinomial measures

A.2.1 General equation of DSI in multinomial measure

We construct a self-similar multinomial measure μ supported by a set \mathcal{F} by a repeated n -based multiplicative cascade, where \mathcal{F} can be an Euclidean set or a fractal set of dimension $\dim \mathcal{F}$. In the first step, the support \mathcal{F} carrying some measure μ is partitioned into n small pieces \mathcal{F}_i with $i = 1, \dots, n$ based on some given set of scale amplification factors

$$\lambda_i = \|\mathcal{F}\| / \|\mathcal{F}_i\|, \quad (\text{A.7})$$

where the measure is redistributed on \mathcal{F}_i according to a set of given multipliers:

$$m_i = \mu(\mathcal{F}_i; r / \lambda_i) / \mu(\mathcal{F}; r). \quad (\text{A.8})$$

In the next step, each piece \mathcal{F}_i is further partitioned into n smaller pieces according to the same amplification factors λ_i and its carrying measure is redistributed again with the same multipliers m_i . This procedure continues *ad* infinity. So far, we have constructed a deterministic self-similar multinomial measure. Define a q -order moment function

$$\Gamma(\mathcal{F}; r, q) = \sum_r \mu^q(\mathcal{F}; r), \quad (\text{A.9})$$

where $\mu(\mathcal{F}; r)$ is the measure in an arbitrary box of scale r and \sum_r represents the sum over all boxes which result from partitioning \mathcal{F} with scale r . When we use boxes of size r to cover \mathcal{F} , the minimum number of disjoint boxes is

$\lceil \lceil \mathcal{F} \rceil / r \rceil$. One finds easily that there might exist a box covering a part of \mathcal{F} whose size is less than r . In this case, we can arrange the $\lceil \lceil \mathcal{F} \rceil / r \rceil$ boxes in a row (like a string) and cover \mathcal{F} in infinitely different ways by translating the boxes string along \mathcal{F} , thus introducing a random “phase.” This phase is one source of noise in the box-counting method. When r is small enough, the noise is reduced greatly so that the moments corresponding to different phases are approximately identical. In other words, the moment function is not affected by the partition procedure and we have

$$\Gamma(\mathcal{F}; r, q) = \sum_{i=1}^n \Gamma(\mathcal{F}_i; r, q) . \quad (\text{A.10})$$

Substitution of Eq. (A.8) in Eq. (A.9) leads to

$$\Gamma(\mathcal{F}_i; r, q) = m_i^q \Gamma(\mathcal{F}; \lambda_i r, q), \quad (\text{A.11})$$

which shows the self-similarity of the moments. Combination of Eqs. (A.10) and (A.11) gives

$$\Gamma(\mathcal{F}; r, q) = \sum_{i=1}^n \Gamma(\mathcal{F}; \lambda_i r, q) m_i^q. \quad (\text{A.12})$$

This is the basic DSI equation of the deterministic self-similar multinomial measures. For statistically self-similar measures [59], Eq. (A.12) can be revised as

$$\Gamma(\mathcal{F}; r, q) = \sum_{j=1}^k \sum_{i=1}^n \Gamma(\mathcal{F}; \lambda_{i,j} r, q) m_{i,j}^q p_j, \quad (\text{A.13})$$

where p_j is the probability of choosing the j -th rule out of the k rules and $\lambda_{i,j}$ and $m_{i,j}$ are accordingly the scaling ratios and measure multipliers [25].

A.2.2 Solution of the DSI equation for lattice multifractals

In the case of $q = 0$, the moment function equals to the number of partitioned boxes $\Gamma(\mathcal{F}; r, 0) = N(\mathcal{F}; r)$, which recovers Eq. (A.3).

If $\lambda_1 = \dots = \lambda_n \equiv \lambda$, it follows from Eq. (A.12) that

$$\Gamma(\mathcal{F}; r, q) = \Gamma(\mathcal{F}; \lambda r, q) \sum_{i=1}^n m_i^q. \quad (\text{A.14})$$

In the formalism of multifractals, one expects that

$$\Gamma(\mathcal{F}; r, q) \propto r^{\tau(q)}, \quad (\text{A.15})$$

where the scaling exponent of the moment is in the form

$$\tau(q) = -\ln \sum_{i=1}^n m_i^q / \ln \lambda. \quad (\text{A.16})$$

In general, the solution to Eq. (A.14) is

$$\Gamma(\mathcal{F}; r, q) = r^{\tau(q)} \psi(r), \quad (\text{A.17})$$

where $\psi(r) = \psi(\lambda r)$ and $\tau(q)$ is defined in Eq. (A.16). Since $\Gamma(\mathcal{F}; 1, q) = 1$, we have $\psi(\lambda^{-\ell}) = 1$, where $\ell \in \overline{\mathbb{Z}^-}$.

Now, consider the case of lattice multifractals with the scale multipliers λ_i satisfying condition (A.4). It follows from (A.12) that

$$\Gamma(\mathcal{F}; r, q) = \sum_{i=1}^n \Gamma(\mathcal{F}; \lambda^{k_i} r, q) m_i^q. \quad (\text{A.18})$$

It is easy to verify that Eq. (A.17) is also the general solution to Eq. (A.18), where $\tau(q)$ is the unique real solution of

$$\sum_{i=1}^n \lambda^{k_i \tau(q)} m_i^q = 1, \quad (\text{A.19})$$

We emphasize that ψ is related to q but independent of λ . Also, the general solution of Eq. (A.13) has the same form of (A.17) with different “ $\tau(q)$ -generation function” in the lattice case.

A.2.3 Oscillations of other characteristic functions of multifractals

It is natural to investigate the presence of oscillations for other functions characterizing multifractals, for instance, the generalized dimensions $D_q(r)$, the strengths of singularity $\alpha(r, q)$, and the multifractal function $f(r, \alpha)$ or $\tilde{f}(r, q)$ [3,4,5,6], when one investigates scaling laws in some experimental data as well as simulated data. Our analysis is performed in terms of the variable r since all these functions vary with r . As usual, we define the exponent function of the moments as

$$\tau(r, q) = d \ln \Gamma(r, q) / d \ln r. \quad (\text{A.20})$$

In equation (A.20), we remove the symbol of the support \mathcal{F} and use $\tau(r, q)$ instead of $\tau(q)$ as is used in [3,4]. Simple algebraic calculations on equation (A.17) leads to

$$\tau(r, q) = \tau(q) + \Psi(r, q), \quad (\text{A.21})$$

where

$$\Psi(r, q) = \frac{r \psi'(r)}{\psi(r)}, \quad (\text{A.22})$$

Similarly, we have

$$D_q(r) \triangleq \lim_{q' \rightarrow q} \frac{\tau(r, q)}{q' - 1} = D_q + \lim_{q' \rightarrow q} \frac{\Psi(r, q')}{q' - 1}, \quad (\text{A.23})$$

$$\alpha(r, q) \triangleq \frac{\partial \tau(r, q)}{\partial q} = \alpha(q) + \frac{\partial \Psi(r, q)}{\partial q}, \quad (\text{A.24})$$

and

$$\tilde{f}(r, q) \triangleq q\alpha(r, q) - \tau(r, q)\tilde{f}(q) + q\frac{\partial \Psi(r, q)}{\partial q} - \Psi(r, q). \quad (\text{A.25})$$

Hence, the four characteristic functions of multifractals, $D_q(r, q)$, $\tau(r, q)$, $\alpha(r, q)$, and $\tilde{f}(r, q)$, are all log-periodic in r with the same period $\ln \lambda$, which is independent of the order q . This result was verified in an experimental situation by extracting the log-periodicity of the moments of the energy dissipation in three-dimensional fully developed turbulence [43]. We shall return to this issue in Sec. A.4.

A.3 DSI in joint multifractal measures

In complex systems, there may be more than one self-similar measure embedded in the same sample space or phase space. For instance, in heated turbulent flow, both the energy dissipation rate ϵ and scalars, say concentration C or temperature T , are known to be multifractal. Thus, it is interesting to consider the joint multifractal measures. Suppose that μ_j with $j = 1, \dots, l$ are l self-similar measures embedded in \mathcal{F} . The joint moments of order $q = \sum_{j=1}^l q_j$ of the l measures are given by

$$J(\mathcal{F}; r, q) = \sum_r \prod_{j=1}^l \mu_j^{q_j}(\mathcal{F}; r). \quad (\text{A.26})$$

The measure multipliers of μ_j are defined by

$$m_{i,j} = \mu_j(\mathcal{F}; r/\lambda_i) / \mu_j(\mathcal{F}; r). \quad (\text{A.27})$$

Combining (A.26) and (A.27), we have

$$J(\mathcal{F}_i; r, q) = J(\mathcal{F}; \lambda_i r, q) \prod_{j=1}^l m_{i,j}^{q_j}. \quad (\text{A.28})$$

It follows from the additive rule of the joint moment

$$J(\mathcal{F}; r, q) = \sum_{i=1}^n J(\mathcal{F}_i; r, q) \quad (\text{A.29})$$

that the DSI equation is

$$J(\mathcal{F}; r, q) = \sum_{i=1}^n J(\mathcal{F}; \lambda_i r, q) \prod_{j=1}^l m_{i,j}^{q_j}, \quad (\text{A.30})$$

for deterministic measures where $\lambda_{i,j}$ and $m_{i,j}$ are the i -th multipliers of μ_j or

$$J(\mathcal{F}; r, q) = \sum_{k=1}^{n'} \sum_{i=1}^n J(\mathcal{F}; \lambda_{i,k} r, q) \prod_{j=1}^l m_{i,j,k}^{q_j} p_k, \quad (\text{A.31})$$

for statistically self-similar measures where $\lambda_{i,k}$ and $m_{i,j,k}$ are i -th multipliers of μ_j for k -th rule with probability p_k .

Similarly, if μ_j satisfy the lattice condition so that $\lambda_{i,k} = \lambda^{k_{i,k}}$, the general solution of Eq. (A.31) is

$$J(\mathcal{F}; r, q) = r^{\tau(q_1, \dots, q_l)} \psi(r), \quad (\text{A.32})$$

where $\psi(r) = \psi(\lambda r)$ and $\tau(q_1, \dots, q_l)$ is the unique real solution of the following equation:

$$\sum_{k=1}^{n'} \sum_{i=1}^n \lambda_{i,k}^{\tau(q_1, \dots, q_l)} \prod_{j=1}^l m_{i,j,k}^{q_j} p_k = 1. \quad (\text{A.33})$$

Again, since $J(\mathcal{F}; 1, q) = 1$, we have $\psi(\lambda^{-\ell}) = 1$, where $\ell \in \overline{\mathbb{Z}^-}$. The deterministic case Eq. (A.30) can be viewed as a special case of Eq. (A.31) with $n' = 1$.

It is clear that the DSI equations of multifractal measures in Sec. A.2 are special cases of those of the joint multifractal measures with $l = 1$. Moreover, their DSI equations are the same in essence despite the possible difference in the coefficients. We expect to confirm the relevance of these formulas in real systems with hierarchical structures, especially in turbulence.

A.4 Complex exponents

The previous sections emphasized the log-periodic structure of lattice fractals and multifractals. However, there is no log-periodicity for the non-lattice case. Instead, we can adopt the more general concept of complex exponents as was done in the former literature [60,34,46]. Indeed, log-periodicity is only a special case of complex exponents in the lattice case, while complex exponents exist for both lattice and non-lattice fractals and multifractals. The complex dimensions of fractal strings were extensively studied from a mathematical view point [60,46]. We note that a fractal string is not identical to the original fractal but to its complement. Hence, we propose a different approach, even for the fractals discussed in the previous sections. In this section, we study the structure of complex exponents in the complex plane and then provide an explicit algorithm for the construction of a sequence of lattice multifractals approximating a non-lattice multifractal whose set of complex exponents is the limit set of the sets of complex exponents of the lattice sequence.

A.4.1 The structure of complex exponents

In the previous sections, we assume that $\tau(q)$ is real, thus the prefactor of the scaling relation $\Gamma(r, q) \propto r^{\tau(q)}$ is a function of r in the lattice case, as expressed in Eq. (A.17). Expanding ψ in the Fourier space yields complex exponents [34]. Therefore, we can assume that $\tau(q)$ is complex so that the prefactor of the scaling relation is independent of r . In this sense, we have

$$\sum_{i=1}^n m_i^q \lambda_i^{\tau(q)} = 1. \quad (\text{A.34})$$

A more general formulae is Eq. (A.33). The solutions of Eq. (A.34) in the complex plane are denoted as

$$\tau(q) = \tau_R(q) + i\tau_I(q), \quad (\text{A.35})$$

where $i = \sqrt{-1}$ is the imaginary unit. We shall study this Eq. (A.34) in the sequel. The results are the same for the stochastic case.

For convenience, let $h(\tau) = \sum_{i=1}^n m_i^q \lambda_i^\tau - 1$. Since $h(-\infty) = \infty$ and $h(\infty) = -1$, and because $h(\tau)$ is continuous, real solutions to (A.34) exist. Moreover, $h(\tau)$ is differentiable and we have $dh(\tau)/d\tau < 0$. Thus Eq. (A.34) has a unique real solution, denoted as $\tau^R(q)$ hereafter. The geometric properties of $\tau^R(q)$ are well-known [6]. As for the complex solutions, it is easy to show from the real value of $h(\tau)$ that, if $\tau(q)$ is a solution to (A.34), then $\bar{\tau}(q) = \tau_R(q) - i\tau_I(q)$ is also a solution. Therefore the set of complex exponents is symmetric with respect to the real axis (the complex exponents come in pairs of complex conjugates).

Let $\tau(q)$ be a solution of Eq. (A.34). Then $\tau_R(q) \geq \tau^R(q)$. Otherwise, by assuming that $\tau_R(q) < \tau^R(q)$, we have $|\sum_{i=1}^n m_i^q \lambda_i^{\tau(q)}| \leq \sum_{i=1}^n m_i^q \lambda_i^{\tau_R(q)} < \sum_{i=1}^n m_i^q \lambda_i^{\tau^R(q)} = 1$. This means that the complex exponents lie on the right of the vertical line $\tau_R(q) = \tau^R(q)$. In the lattice case, $\tau(q) = \tau^R(q) + in\omega$ also belong to the set of complex exponents, where $n \in \mathbb{Z}$ and $\omega = 2\pi/\ln \lambda$ is the fundamental angular log-frequency of lattice fractals and multifractals. In the non-lattice case, $\tau(q) = \tau^R(q)$ is the only complex exponent satisfying $\tau_R(q) = \tau^R(q)$. Furthermore, there is a right boundary $\tau_0(q)$ of the set of complex exponents, that is, $\tau_R(q) < \tau_0(q)$. (We refer the interested reader to Sec. 2.5 of [46] for a rigorous proof for fractal strings, which can be easily generalized to the present case.) Hence the set of complex exponents lie in a strip $[\tau^R(q), \tau_0(q)] \times \mathcal{R}$.

In the case of lattice multifractal, there exists a preferred scaling ratio λ so that equation (A.34) can be expressed as a polynomial equation (A.19) with respect to the unknown $\lambda^{\tau(q)}$ of degree $\max_j \{k_j\}$. The set of complex exponents is obtained easily from the set of complex solutions of (A.19). Hence there are

finite complex numbers $\tau_j(q)$ such that the set of complex exponents is given by

$$\mathcal{T} = \{\tau_j(q) + in\omega, \ n \in \mathcal{Z}, \ j = 1, 2, \dots, \ell\}, \quad (\text{A.36})$$

where $\ell \leq \max_j \{k_j\}$. Thus the complex exponents lie on finitely many vertical lines in the complex plane. The points on each vertical line corresponding to a given $\tau_j(q)$ are distributed evenly with spacing ω .

Assume that $(\tau_j)_R \neq (\tau_k)_R$ for $j \neq k$ and $\tau_1(q) = \tau^R(q)$. Then we have

$$(\tau_j)_I = \omega/2, \quad (\text{A.37})$$

where $j > 1$. This result derives because the points on each line are evenly located with spacing ω and symmetric with respect to the real axis. The log-frequencies of the moments are thus given by

$$f_{j,n} = \frac{(\tau_j)_I + n\omega}{2\pi} = \begin{cases} n\omega/2\pi, & \text{if } j = 1 \\ (\frac{1}{2} + n)\omega/2\pi, & \text{if } j > 1 \end{cases}, \quad (\text{A.38})$$

where $n \in \mathcal{Z} - \{0\}$ when $j = 1$ and $n \in \mathcal{Z}$ when $j > 1$, $f_{1,1}$ is the fundamental log-frequency and $f_{j>1,0}$ are subharmonics of $f_{1,1}$ [40]. Certainly, it is also possible that there are at least two complex exponents with indices j and k such that $(\tau_j)_R = (\tau_k)_R$. In this case, the points on the line $\tau_R(q) = (\tau_k)_R$ are no longer evenly spaced with period ω . This possibility will be clearer in the following when we approximate a non-lattice multifractal with a sequence of lattice multifractals. It is clear that $f_{j>1,0}$ might change for different orders q . Nevertheless, $f_{1,1} = \omega/2\pi$ holds for any q . In other words, the fundamental log-frequency of a lattice multifractal is independent of the order q [43].

In the case of non-lattice multifractals, the set of complex exponents is not periodic. However, the necessary and sufficient condition for the existence of log-periodicity is the existence of periodicity in the plane of the complex exponents associated with a preferred scaling ratio. In the present case, there is no such preferred scaling ratio and hence no log-periodicity. The complex exponents of a non-lattice multifractal can be approximated by the complex exponents of a sequence of lattice multifractals with larger and larger ω . The approximation sequence of lattice multifractals can be constructed explicitly, as in the case of fractal strings [46]. This construction process is described in the following Sec. A.4.2.

A.4.2 Approximating non-lattice multifractal by a sequence of lattice multifractals

Let us denote the scaling ratios Λ of the non-lattice multifractal as λ_j where $j = 1, \dots, n$. Given any real number $\lambda_0 > 1$, we have a set of numbers

$\Theta = \{\theta_j = \ln \lambda_j / \ln \lambda_0 : j = 1, \dots, n\}$, defining the coordinates of a point in the n dimensional space \mathcal{R}^n . Since the multifractal is non-lattice, there is at least one j such that θ_j is an irrational number for any possible choice of λ_0 . It is known that there exists a sequence of points $\Theta^{(k)} = \{\theta_j^{(k)} : j = 1, \dots, n\} \in \mathcal{R}^n$ which converge to Θ , where $\theta_j^{(k)}$ are rational numbers. Obviously, the sequence of rational numbers $\theta_j^{(k)}$ converge to θ_j for every $j = 1, \dots, n$. If some θ_j is rational, we stipulate trivially that $\theta_j^{(k)} = \theta_j$ for all k . Posing $\lambda_j^{(k)} = \lambda_0^{\theta_j^{(k)}}$, we obtain a sequence of lattice multifractals $\Lambda^{(k)}$ with scaling ratios $\{\lambda_j^{(k)} : j = 1, \dots, n\}$ converging to the non-lattice multifractal. The set of complex exponents $\mathcal{T}^{(k)}$ of $\Lambda^{(k)}$ converges to the set of complex exponents \mathcal{T} of Λ . In practice, we can take a lattice multifractal $\Lambda^{(k)}$ with k large enough as an approximation of the non-lattice multifractal Λ .

Let us write $\theta_j^{(k)} = s_j^{(k)} / t_j^{(k)}$ where $s_j^{(k)}$ and $t_j^{(k)}$ are relatively prime. Let $t^{(k)}$ be the minimal common divisor of $\{t_j^{(k)} : j = 1, \dots, n\}$. Then $\lambda^{(k)} = \lambda_0^{1/t^{(k)}}$ is the preferred scaling ratio of $\Lambda^{(k)}$. We thus recover the polynomial equation (A.19):

$$\sum_{j=1}^n m_j^q \left[\lambda_0^{\tau(q)/t^{(k)}} \right]^{s_j^{(k)} t^{(k)} / t_j^{(k)}} = 1, \quad (\text{A.39})$$

where $s_j^{(k)} t^{(k)} / t_j^{(k)}$ are integers. We can choose a sequence ensuring that $\theta_j^{(k)}$ is monotonous with respect to k . It follows that $t^{(k)}$ increases with k . Therefore, the fundamental log-frequencies $f^{(k)} = 1 / \ln \lambda^{(k)}$ of $\Lambda^{(k)}$ increase when converging to Λ . In other words, there is no finite limit of $f^{(k)}$ when k tends to ∞ and the fundamental log-frequency of a non-lattice multifractal is thus not defined. Practically, when one investigates the Lomb periodogram of the residuals of a q -order moment of a non-lattice multifractal, the log-frequency corresponding to the highest Lomb peak is indefinite and increases when the sampling of data points of the moment becomes denser (so as to investigate more scales r) [43]. On the other hand, the distance of separation between the complex exponents on each vertical line becomes larger and larger. This is not surprising since the degree $\max_j \{s_j^{(k)} t^{(k)} / t_j^{(k)}\}$ of the polynomial equation (A.39) increases with k implying more vertical lines, some of which may overlap.

References

- [1] Mandelbrot, BB. The Fractal Geometry of Nature. New York: W. H. Freeman, 1983.
- [2] Mandelbrot, BB. Intermittent turbulence in self-similar cascade: Divergence of high moments and dimension of carrier. J Fluid Mech 1974;62:331–358.

- [3] Grassberger, P. Generalized dimensions of strange attractors. *Phys Lett A* 1983;97:227–230.
- [4] Hentschel, HGE, Procaccia, I. The infinite number of generalized dimensions of fractals and strange attractors. *Physica D* 1983;8:435–444.
- [5] Frisch, U, Parisi, G. On the singularity structure of fully developed turbulence. In: M Gil, R Benzi, G Parisi, eds., *Turbulence and Predictability in Geophysical Fluid Dynamics and Climate Dynamics*. Amsterdam, North-Holland: Elsevier, 1985; pp. 84–88.
- [6] Halsey, TC, Jensen, MH, Kadanoff, LP, Procaccia, I, Shraiman, BI. Fractal measures and their singularities: The characterization of strange sets. *Phys Rev A* 1986;33:1141–1151.
- [7] Lee, J, Stanley, HE. Phase transition in the multifractal spectrum of diffusion-limited aggregation. *Phys Rev Lett* 1988;61:2945–2948.
- [8] Blumenfeld, R, Aharrony, A. Breakdown of multifractal behavior in diffusion-limited aggregation. *Phys Rev Lett* 1989;62:2977–2980.
- [9] Schwarzer, S, Lee, J, Bunde, A, Halvin, S, Roman, HE, Stanley, HE. Minimum growth probability of diffusion-limited aggregation. *Phys Rev Lett* 1990;65:603–606.
- [10] Mandelbrot, BB. New “anomalous” multiplicative multifractals: Left sided $f(\alpha)$ and the modelling of DLA. *Physica A* 1990;168:95–111.
- [11] Mandelbrot, BB, Evertsz, CJG, Hayakawa, Y. Exactly self-similar left-sided multifractal measures. *Phys Rev A* 1990;42:4528–4536.
- [12] Riedi, RH. An improved multifractal formalism and self-similar measures. *J Math Anal Appl* 1995;189:462–490.
- [13] Riedi, RH, Mandelbrot, BB. Multifractal formalism for infinite multinomial measures. *Adv Appl Math* 1995;16:132–150.
- [14] Falconer, KJ, O’Neil, TC. Vector-valued multifractal measure. *Proc Royal Soc A* 1996;452:1433–1457.
- [15] Zhou, WX, Yu, ZH. On the properties of random multiplicative measures with the multipliers exponentially distributed. *Physica A* 2001;294:273–282.
- [16] Zhou, WX, Liu, HF, Yu, ZH. Anomalous features arising from random multifractals. *Fractals* 2001;9:317–328.
- [17] Huillet, T, Porzio, A. On continuously-generated self-similar multifractals. *Fractals* 2001;9:129–147.
- [18] Zhou, WX, Yu, ZH. Multifractality of drop breakup in the air-blast nozzle atomization process. *Phys Rev E* 2001;63:016302.
- [19] Mandelbrot, BB. Multifractal measures, especially for the geophysicist. *Pure Appl Geophys* 1989;131:5–42.

- [20] Mandelbrot, BB. Negative fractal dimensions and multifractals. *Physica A* 1990;163:306–315.
- [21] Mandelbrot, BB. Random multifractals: Negative dimensions and the resulting limitations of the thermodynamic formalism. *Proc Royal Soc A* 1991;434:79–88.
- [22] Cates, M, Witten, T. Diffusion near absorbing fractals: Harmonic measure exponents for polymers. *Phys Rev A* 1987;35:1809–1834.
- [23] Chhabra, AB, Sreenivasan, KR. Negative dimensions: Theory, computation and experiment. *Phys Rev A* 1991;43:1114–1117.
- [24] Chhabra, AB, Sreenivasan, KR. Scale-invariant multiplier distribution in turbulence. *Phys Rev Lett* 1992;68:2762–2765.
- [25] Zhou, WX, Yu, ZH. Does randomness in multinomial measures imply negative dimensions. In: MM Novak, ed., *Emergent Nature: Patterns, Growth and Scaling in the Sciences*. Singapore: World Scientific, 2002; pp. 434–435.
- [26] Olsen, L. Measurability of multifractal measure functions and multifractal dimension functions. *Hiroshima Math J* 1999;29:435–458.
- [27] Olsen, L. Multifractal geometry. *Progress in Probability* 2000;46:3–37.
- [28] Bessis, D, Geronimo, JS, Moussa, P. Complex spectral dimensionality on fractal structures. *J Phys Lett* 1983;44:977–982.
- [29] Badii, R, Politi, A. Intrinsic oscillations in measuring the fractal dimension. *Phys Lett A* 1984;104:303–305.
- [30] Smith, LA, Fournier, JD, Spiegel, EA. Lacunarity and intermittency in fluid turbulence. *Phys Lett A* 1986;114:465–468.
- [31] Bessis, D, Fournier, JD, Servizi, G, Turchetti, G, Vaienti, S. Mellin transform of correlation integrals and generalized dimension of strange sets. *Phys Rev A* 1987;36:920–928.
- [32] Bessis, D, Servizi, G, Turchetti, G, Vaienti, S. Mellin transforms and correlation dimensions. *Phys Lett A* 1987;119:345–347.
- [33] Fournier, JD, Turchetti, G, Vaienti, S. Singularity spectrum of generalized energy integrals. *Phys Lett A* 1989;140:331–335.
- [34] Sornette, D. Discrete scale invariance and complex dimensions. *Phys Rep* 1998; 297:239–270.
- [35] Johansen, A, Sornette, D. Evidence of discrete scale invariance in DLA and time-to-failure by canonical averaging. *Int J Modern Phys C* 1998;9:433–447.
- [36] Johansen, A, Sornette, D. Critical ruptures. *Eur Phys J B* 2000;18:163–181.
- [37] Zhou, WX, Sornette, D. Generalized q -analysis of log-periodicity: Applications to critical ruptures. *Phys Rev E* 2002;66:046111.

- [38] Johansen, A, Saleur, H, Sornette, D. New evidence of earthquake precursory phenomena in the 17 Jan. 1995 Kobe earthquake, Japan. *Eur Phys J B* 2000; 15:551–555.
- [39] Huang, Y, Saleur, H, Sornette, D. Reexamination of log-periodicity observed in the seismic precursors of the 1989 Loma Prieta earthquake. *J Geophys Res* 2000;105:28111–28123.
- [40] Sornette, D, Johansen, A, Arneodo, A, Muzy, JF, Saleur, H. Complex fractal dimensions describe the internal hierarchical structure of DLA. *Phys Rev Lett* 1996;76:251–254.
- [41] Novikov, EA. The effects of intermittency on statistical characteristics of turbulence and scale similarity of breakdown coefficients. *Phys Fluids A* 1990; 2:814–820.
- [42] Johansen, A, Sornette, D, Hansen, AE. Punctuated vortex coalescence and discrete scale invariance in two-dimensional turbulence. *Physica D* 2000; 138:302–315.
- [43] Zhou, WX, Sornette, D. Evidence of intermittent cascades from discrete hierarchical dissipation in turbulence. *Physica D* 2002;165:94–125.
- [44] Sornette, D. *Why Stock Markets Crash: Critical Events in Complex Financial Systems*. Princeton: Princeton University Press, 2003.
- [45] Zaslavsky, G. Multifractal kinetics. *Physica A* 2000;288:431–443.
- [46] Lapidus, M, Van Frankenhuysen, M. *Fractal Geometry and Number Theory: Complex Dimensions of Fractal Strings and Zeros of Zeta Functions*. Boston: Birkhäuser, 2000.
- [47] Mandelbrot, BB. A class of multinomial multifractal measures with negative (latent) values for the “dimension” $f(\alpha)$. In: L Pietronero, ed., *Fractals’ Physical Origin and Properties*, pp. 3–29. New York: Plenum, 1989;.
- [48] Horne, JH, Baliunas, SL. A prescription for period analysis of unevenly sampled time series. *Astrophys J* 1986;302:757–763.
- [49] Press, W, Teukolsky, S, Vetterling, W, Flannery, B. *Numerical Recipes in FORTRAN: The Art of Scientific Computing*. Cambridge: Cambridge University Press, 1996.
- [50] Zhou, WX, Sornette, D. Statistical significance of periodicity and log-periodicity with heavy-tailed correlated noise. *Int J Modern Phys C* 2002;13:137–170.
- [51] Sornette, D. Discrete scale invariance in turbulence? In: U Frisch, ed., *Proceedings of the Seventh European Turbulence Conference*. Kluwer, 1998; .
- [52] Meneveau, C, Sreenivasan, KR. Simple multifractal cascade model for fully developed turbulence. *Phys Rev Lett* 1987;59(5):1424–1427.

- [53] Ball, RC, Witten, TA. Particle aggregation versus cluster aggregation in high dimensions. *J Stat Phys* 1984;36:873–879.
- [54] Witten, TA, Cates, ME. Tenuous structure from disorderly growth processes. *Science* 1986;232(4758):1607–1612.
- [55] Arnéodo, A, Argoul, F, Bracy, E, Muzy, JF. Golden mean arithmetic in the fractal branching of diffusion-limited aggregates. *Phys Rev Lett* 1992;68:3456–3459.
- [56] Arnéodo, A, Argoul, F, Muzy, JF, Tabard, M. Uncovering fibonacci sequences in the fractal morphology of diffusion-limited aggregates. *Phys Lett A* 1992; 171:31.
- [57] Arnéodo, A, Argoul, F, Muzy, JF, Tabard, M, Bracy, E. Beyond classical multifractal analysis using wavelets: Uncovering a multiplicative process hidden in the geometrical complexity of diffusion limited aggregates. *Fractals* 1993; 1:629.
- [58] Grassberger, P, Procaccia, I. Measuring the strangeness of strange attractors. *Physica D* 1983;9:189–208.
- [59] Falconer, KJ. The multifractal spectrum of statistically self-similar measures. *J Theor Probab* 1994;7:681–702.
- [60] Makarov, KA. Asymptotic expansions for Fourier transform of singular self-affine measures. *J Math Anal Appl* 1994;186:259–286.